

# Prediction of welding sequence induced thermal history and residual stresses and their effect on welding distortion

Arpan Kumar Mondal<sup>1,2</sup> · Pankaj Biswas<sup>1</sup> · Swarup Bag<sup>1</sup>

Received: 7 September 2015 / Accepted: 3 April 2017 / Published online: 25 April 2017  
© International Institute of Welding 2017

**Abstract** Stiffened plate panel is the major structural part of a fabrication industry where fillet welding joint is one of the most important fabrication techniques. Large stiffened structures are generally joined by several welding passes which generates thermal stresses and angular deformation. Tensile residual stresses which are generated due to welding in the weld region may lead to early failure of the structure when subjected to cyclic loading. The weld-induced residual distortion causes dimensional inaccuracy and needs rework to achieve the desired shape. Use of multiple welding passes without any optimized welding sequences typically leads to an increased degree of nonuniform heating and cooling, i.e., creating complex welding residual stress and angular deformation in the structure. In this present study, the effect of four different welding sequences on submerged arc welded fillet joint has been studied. A finite element-based numerical model has been developed to predict the thermal profile, welding residual stress, and angular deformation. The developed model considers temperature-dependent material property and material deposition by using element death and birth technique. The results have been compared with experimental one. In the effect of welding sequence on residual stress, angular deformation has been studied. Thus, the developed model presents the effect of welding sequence on the weld induced residual stresses and

distortions which provide one of the most optimal welding sequence for enhanced fabrication process.

**Keywords (IIW Thesaurus)** Finite element analysis · Element death and birth · Plastic strain · Welding residual distortion · Stiffened panel · Fillet joint

## 1 Introduction

Large structures are made by assembling different small components which joined together by several welding passes. Any large structure like ships and bridges contain huge number of stiffener joints. It has been observed that welding sequences have significant effect on welding induced residual stresses and angular deformation. The ship hull girder consists of several stiffened panels where several welding passes are required for fabrication; here, welding pass plays a very crucial role on the weld-induced residual stress and angular deformation. As the means of welding is fusion, the welding heat source is sufficient to melt the electrode and the base metal to join the components together; thus, the local heating produces enormous thermal gradient and non-uniform cooling of the base metal produces thermal stresses followed by residual stress and deformation. The material near to the weld zone reaches to plastic state due to thermal strain which causes the development of shrinkage forces to lead to the angular distortion of the welded joint [1].

Angular distortion in a welded structure also results from the high thermal gradients followed by high expansion and contraction of the weld metal and the neighboring base metal during the heating and cooling process of the welding. Due to higher temperature difference with the surrounding, the molten metal at the weld zone gets cooled and shrinks much faster than the surrounding base metal. When several pass of welding is done after one pass, the adjacent base metal gets preheated. The controlled

---

Recommended for publication by Commission X - Structural Performances of Welded Joints - Fracture Avoidance

---

✉ Arpan Kumar Mondal  
m.arpan@iitg.ernet.in

<sup>1</sup> Department of Mechanical Engineering, Indian Institute of Technology Guwahati, Guwahati, Assam 781039, India

<sup>2</sup> Department of Mechanical Engineering, National Institute of Technical Teachers' Training & Research Kolkata, Kolkata, West Bengal 700106, India

welding sequences can take the benefit of preheating done by the previous pass and can minimize the temperature gradient between weld zone and neighboring metal. This results in more uniform or controlled heating and cooling which results in less shrinkage, i.e., less angular distortion.

In the present study, a fusion welding process, i.e., submerged arc welding (SAW) is considered. SAW has a wide range of voltage, current, material deposition with around 95% thermal efficiency, and automatic controllability. Mostly large stiffened structures involve several welding passes with no specific welding sequence. After a weld pass is finished, the nearby material gets preheated; thus, less heat should be supplied to weld that part. Optimized welding sequence will control the amount of heat available to melt the material; hence, the final amount of residual stress and deformation can be minimized. Weld-induced residual stress and distortions have been found to reduce the strength of the stiffened panels of ship structures [2–4]. Deformed structures often followed by necessary costly rework like postweld heat treatment and cold bending [2] of the misaligned parts to reduce the distortion at a tolerable level thus increasing the production time and cost.

As the fusion welding process involves rapid heating and cooling, it is difficult to measure the weld thermal profile. Knowledge of thermal history is essential for the estimation of the final residual stress and deformation of the welded sample. Several researchers introduced mathematical and process models of the fusion welding phenomena in the recent past [1–5, 7–9].

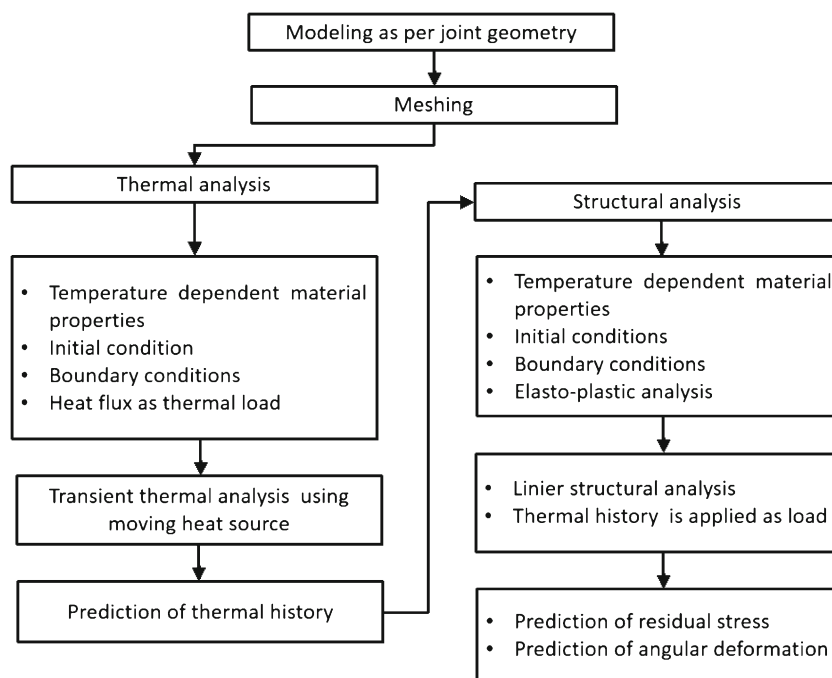
Use of FEM to investigate the heat transfer characteristics has been reported by many researchers [6, 20, 21]. Some researchers [22–24] also estimated the heat source model parameters for different fusion welding processes. Wen et al. [20] used FEM to investigate the heat transfer characteristics and effect of different weld parameters on residual stress and deformation; they also compared the numerical and experimental results and a good agreement between the same was reported. Fanous et al. [17] presented a 3-D finite element modeling where they introduced element death and birth technique to take care the material deposition. Numerical simulation was reported by researchers [26] to study the effect of process parameters of residual stress and angular deformation in submerged arc welded butt joint. Investigation of the residual stress and distortion of single sided [14] as well as double-sided [27] fillet joints were also reported. Malik et al. [21] presented a numerical model to study the temperature distribution and prediction of fusion zone (FZ) and heat-affected zone (HAZ) in gas tungsten arc welding (GTAW). Adak et al. [28] tried to predict the effects of different restraints on the weld-induced residual deformations and stresses in a steel plate; they have also studied the effect of weld parameters on the temperature-time history [29]. Liang et al. [33] experimentally and numerically investigated the residual stress in multi-pass thick plate joint welded by GTAW.

Among the recent researchers, Yadhav et al. [5] and Podder et al. [13] introduced new heat source models for the

numerical simulations of the fusion welding processes. Nart and Celik [30] used Goldak's double ellipsoidal heat source model to simulate the submerged arc welding process. Jiang et al. [31] and Zhao et al. [37] are among the new researchers who contributed towards the simulation of the SAW process. Kiran et al. [34] reported to use a charge-coupled device (CCD) camera to know the arc behavior of SAW process extensively. Considering the effect of different welding parameters and flux [32] on the mechanical properties of the final part, numerous researchers have attempted to address the issue extensively. The work in the direction of studying the effect of different weld parameters on residual stress and deformation and prediction of FZ and HAZ was also reported by several researchers [20–31, 37]. The effect of heat input [38, 39] on weld bead geometry of SAW process was also reported.

Some researchers [7–9, 15, 16, 40] investigated thermoelastic plastic analysis for predicting residual stresses and distortions. Researchers studied the distortion mechanism [7, 8] and predicted the effect of process parameters and welding sequence [9, 10] on distortion and residual stress of large structures. Kohandehghan [11] reported experimental investigation on effect of welding sequence on residual stress using arc welding process. Attempt has been made to study the residual stress and distortions of T-joint fillet weld [12] and effect of welding sequence on residual stress on multi-pass welding joint [9]. Researchers developed and implemented various methods like eigenstrain reconstruction method [42] and average plastic strain method [1] for predicting the deformations in large structures.

In a nutshell, a large number of numerical models are available to effectively estimate the thermal and structural behavior in a SAW process. The objective of the work is to use these techniques to study the effect of welding sequence manipulation on residual stress and angular deformation of a small part welded by submerged arc welding (SAW). This may be further implemented for large structures. Optimal welding sequence manipulation will control the preheating effect, while welding in one side of the fillet tensile stress will be developed in the weld side but compressive stress will develop in the opposite side. Efficient control of weld passes will superimpose the residual stress developed in either pass, which may lead to the mitigation of the residual stresses and distortion. A three-dimensional finite element model has been developed to predict the effect of four different welding sequences on angular deformation and residual stress. During modeling, the effect of temperature-dependent material properties and material deposition has been taken care of. Four different welding sequences have been studied using coupled thermomechanical elasto-plastic finite element analysis. Thermal history has been successfully predicted and validated with experiment for all welding sequences. It has been found that the developed model can successfully predict the angular deformation and residual stress for different welding sequences.

**Fig. 1** 3-D sequential coupled thermomechanical analysis

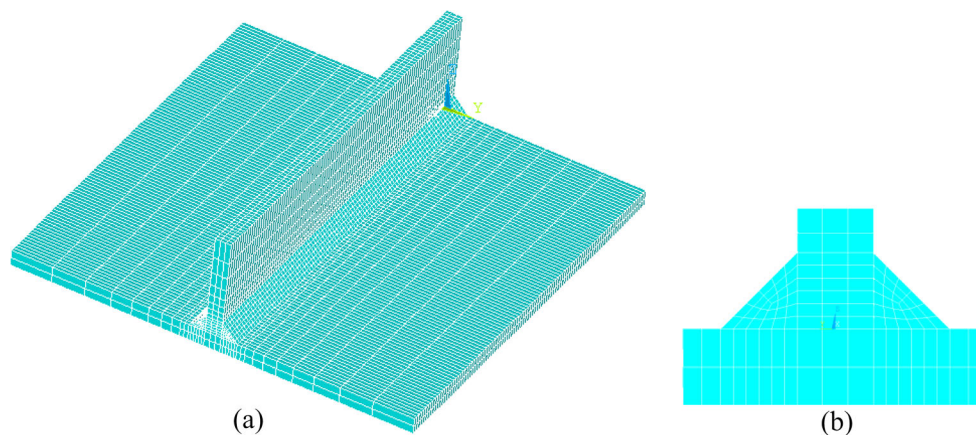
## 2 Modeling methodology

3-D transient elasto-plastic thermomechanical finite element (FE) model considering the temperature-dependent material properties was developed to simulate the residual stress and angular deformation. Density of the material was considered constant. Linear Newtonian convective cooling was assumed. No forced convection was considered. Convective cooling was assumed in all the surfaces except the weld zone. The solution was done in the ANSYS 14 finite element package. The overall FE procedure is shown in the Fig. 1.

For finding out the residual stress and angular deformation distribution pattern over the entire welded plate for four different welding sequences were studied, first of all, transient thermal analysis was carried out to find out the nodal transient temperatures. The second part of the nonlinear elasto-plastic analysis was done

by using the result obtained from the transient thermal analysis with consideration of the temperature-dependent thermal and mechanical material properties, moving heat source, material deposition, elastic-plastic behavior of the base material and joint geometry. For 3-D FE modeling and analysis, eight noded brick elements were used for the thermal analysis and similar eight noded elements were used in the structural analysis. The total numbers of nodes and elements in the meshed model were 22,712 and 16,800, respectively. The mesh density was finalized after mesh sensitivity analysis, keeping a balance between the computation time and prediction accuracy. The meshed view of the model is shown in the Fig. 2.

Figure 2 represents the meshed view of the fillet model with stiffener. Here, nonuniform meshing has been applied to save the computation time. The mesh size gradually increases from the center of the weld line to away from the weld

**Fig. 2** a Meshed view of the model. b Cross-sectional view

line. The welding parameters are given in Table 5 which were considered for analyzing the welding operation of the fillet joint.

### 2.1 Thermal analysis

Figure 4 shows the schematic representation of the fillet joint with three-dimensional plates to be welded by submerged arc welding. The governing equation of the submerged arc welding process is the standard Fourier's law of heat conduction equation.

$$\rho c \frac{\partial T}{\partial t} = \frac{\partial}{\partial x} \left[ k_x \frac{\partial T}{\partial x} \right] + \frac{\partial}{\partial y} \left[ k_y \frac{\partial T}{\partial y} \right] + \frac{\partial}{\partial z} \left[ k_z \frac{\partial T}{\partial z} \right] + q \quad (1)$$

where  $\rho$  is the density and  $c$  is the specific heat of mild steel;  $T$  is the instantaneous temperature at any point at time  $t$  in the domain  $T = T(x, y, z, t)$ ; and  $k_x$ ,  $k_y$ , and  $k_z$  are the thermal conductivities of the material at  $x$ ,  $y$ , and  $z$  directions, respectively. But as the mild steel plate is homogeneous, isotropic material properties have been considered; therefore,  $k_x = k_y = k_z = K$ .  $q$  is the input; generally, submerged arc welding heat input can be considered as the Gaussian distributed heat source [30, 31, 19].

Considering a Gaussian distribution of power density due to the submerged welding arc, the heat flux  $q$  of the moving heat source, on the top surface of the workpiece, is expressed as

$$q = \frac{3Q}{\pi r^2} \exp \left[ -3 \left( \frac{R}{r} \right)^2 \right] \quad (2)$$

where  $Q = \eta VI =$  heat input (W),  $V =$  voltage (V),  $I =$  current (A), and  $\eta =$  the welding efficiency.  $R$  is the distance from the center of the heat source on the plate surface; " $r$ " is the characteristic radial dimensional distribution parameter that defines the region in which 95% of heat flux is deposited [23]. In the present study, the value of  $r$  is 5 mm. As in the case of SAW, the weld zone is submerged under the flux; convection head loss is assumed all over the plate except the weld zone.

The initial conditions and boundary conditions were applied accordingly. Before the start of welding, the initial uniform plate temperature was set to room ambient temperature. During welding and cooling, heat loss is considered from convection and the radiation heat loss was ignored. The boundary condition was applied to free surfaces of the plate exposed to the ambient temperature except the welding zone. The heat loss flux was applied as the following.

$$q_s = -h_f(T_s - T_a) \quad (3)$$

where  $q_s$  is the convective heat loss,  $h_f$  is the convective heat transfer coefficient,  $T_s$  is the surface temperature, and  $T_a$  is the ambient temperature. A constant convection coefficient of  $15 \text{ W/m}^2 \text{ K}$  was considered [18, 43].

### 2.2 Structural analysis

The stress-strain relationship from Hook's law can be represented as

$$\sigma = D \varepsilon_e \quad (4)$$

where  $\sigma$  is residual stress,  $\varepsilon_e$  is elastic strain, and  $D$  is stress modulus.

The elastic strain is given as

$$\varepsilon_e = \varepsilon - \varepsilon_{pl} - \varepsilon_{th} \quad (5)$$

where  $\varepsilon_e =$  the elastic strain,  $\varepsilon =$  total strain,  $\varepsilon_{pl} =$  plastic strain vector, and  $\varepsilon_{th} =$  thermal strain.

The structural analysis involved large displacements (strain) which consists plastic, elastic, and thermal parts; therefore, thermoelasto-plastic material model is used. The elastic behavior of welded metal was modeled with isotropic Hook's Law considering temperature-dependent material properties (Young's modulus and Poisson's ratio). To incorporate the plastic behavior, rate-independent thermoelasto-plastic material model was applied. Welding residual stress is greatly influenced by strain hardening; therefore, bilinear kinematic hardening model was used while von-Mises yield criterion was considered as the yield criterion [14, 44, 45]. Although annealing effect has an influence on residual stress, it was not taken into account to reduce further complexity.

### 2.3 Material deposition using element death and birth method

During submerged arc welding operation, filler material is added from the continuous electrode. The finite element modeling is performed considering the filler material addition. With the moving heat source, extra material is added to consider the filler material deposition at the weld joint. To take care of the filler material element, birth and death techniques have been used.

In practice, no element is deleted or eliminated by the software; in fact, the dead materials are deactivated during the simulation process. The proposed method does not remove elements to achieve the "death" effect. Instead, the method deactivates an element by multiplying its stiffness by a large reduction factor. The deactivation of the dead materials is performed by multiplying their stiffness to a severe reduction factor where in general the default value is  $10^{-6}$  [41]. The mass and energy of deactivated elements are excluded from the summations of model. An element's strain is also set to zero as soon as that element is killed. Similarly, when elements are "born," they are not actually added to the model, but are simply reactivated. The geometrical nonlinearity option is activated to take care of the deformation of the material in all the subsequent loading before and after the birth of the material. While activating the dead materials upon removing

**Table 1** Temperature-dependent material properties of mild steel [18]

Temperature (°C)	Thermal Conductivity (W/m K)	Specific heat (J/kg K)	Thermal expansion coefficient ( $10^{-6}/^{\circ}\text{C}$ )	Young modulus (GPa)	Poisson ratio
0	51.9	450	10	200	0.2786
100	51.1	499.2	11	200	0.3095
300	46.1	565.5	12	200	0.331
450	41.05	630.5	13	150	0.338
550	37.5	705.5	14	110	0.3575
600	35.6	773.3	14	88	0.3738
720	30.64	1080.4	14	20	0.3738
800	26	931	14	20	0.4238
1450	29.45	437.93	15	2	0.4738
1510	29.7	400	15	0.2	0.499
1580	29.7	735.25	15	0.00002	0.499
3500	42.1	400	15.5	0.00002	0.499

the reduction factor, all the process variables (its stiffness, mass, element loads, etc.) also restored to their original values [17, 25, 35], which are known as the birth of the materials.

## 2.4 Material properties

The temperature-dependent material properties of mild steel (MS) used for the transient heat transfer analysis and elastoplastic analysis are given in Table 1. Temperature-dependent enthalpy and yield stress for mild steel are given in Tables 2 and 3, respectively. The melting and transformation temperature of MS are 1495 and 723 °C, respectively.

## 3 Experimental details

An ADORE SAW setup was used to perform the welding of samples with four welding sequences. Copper-coated mild steel electrode of 3.1 mm diameter and ESAB OK FLUX

10.17 L granular flux have used for carrying out the experiments. Temperature data was recorded by using Agilent data logger. K-type thermocouples were used as the temperature sensor. Thermocouples were fixed perpendicular to the weld line. A schematic diagram of the thermocouple arrangements is represented in the Fig. 3c. Figure 3 a, c shows the welded sample with attached thermocouples and the welding setup, respectively. A coordinate measuring machine (CMM) was used to measure the angular deformation of the plates before and after welding which is shown in the Fig. 3d.

The welding parameters used in present study are shown in Table 5. In the present analysis, a double-sided fillet welding was considered. The plate used in this study is an 8 mm thick 200 mm × 200 mm mild steel plate with a stiffener with a web height of 50 mm and thickness 8 mm.

The range levels of the process variables can be seen in the Table 4. To find the range of parameters, trial and error experiments were conducted with wide range of the process variable, where only one parameter was varied at a time instant and the other two were kept constant. To find the accurate process parameter settings which give the best weld bead geometry, Taguchi [36] L9 design of experiment has been performed with three process variables current, voltage, and welding speed where the length of stick out was kept at a constant value of 2.5 mm (Fig. 4). The weld bead dimensions were taken as the output characteristics, while the throat size of the fillet was kept as 0.7 times of the leg length for the best weld bead. The optimized parameters using the Taguchi design of experiment is used in the numerical analysis as shown in the Table 5.

To study the effect of welding sequences on residual stress and deformation, welding is done according to different welding sequences as described in the following Table 6 as per Fig. 3.

## 4 Results and discussions

In the present study, both thermal and mechanical analyses were performed. Experiments were conducted to validate the model. Figure 5a–d shows the results of the time-temperature

**Table 2** Temperature-dependent enthalpy for mild steel [18]

Temperature (°C)	0	100	200	300	400	500	600	700	800	900	1000	>2500
Enthalpy (MJ/m <sup>3</sup> )	0	360	720	1100	1500	1980	2500	3000	3700	4500	5000	9000

**Table 3** Temperature-dependent yield stress for mild steel [18]

Temperature (K)	293	373	573	773	973	1073	1273	1473	1673
Yield stress ( $\sigma_y$ ) (MPa)	398	379	305	192	41	36	28	20	12

**Fig. 3** **a** Welded plate. **b** Thermocouple arrangements. **c** Welding setup. **d** Angular deformation measurement using CMM

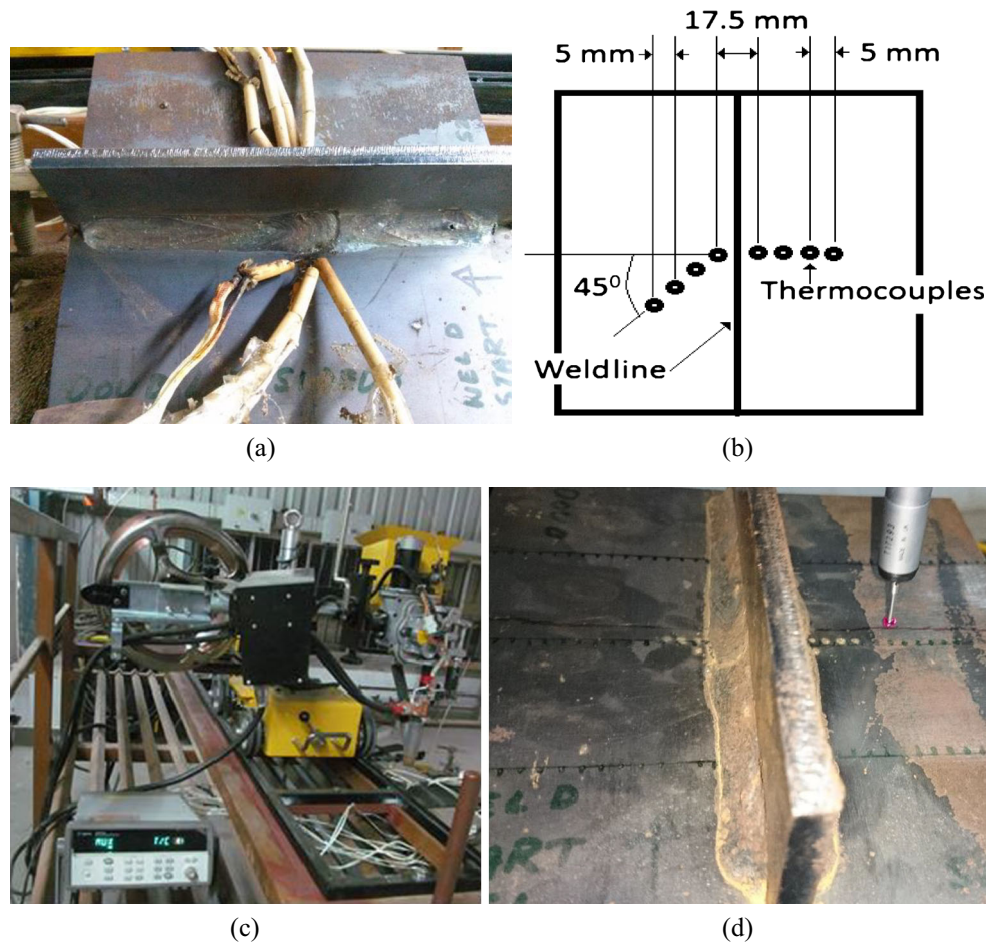


**Table 4** Range of the welding parameters used in the trial and error experiments

Current (A)	Voltage (V)	Welding speed (m/s)
450–550	20–35	0.003–0.009

history of the submerged arc welding for four different welding sequences, i.e., WS-I, WS-II, WS-III, and WS-IV, respectively. Transient temperature distribution of two different locations for each welding sequence has been compared. The experimental thermal history of the welded plate for all four welding sequences was captured by K-type thermocou-

**Table 5** Welding parameters used in numerical analysis

Current (A)	Voltage (V)	Welding speed (m/s)
490	25	0.005

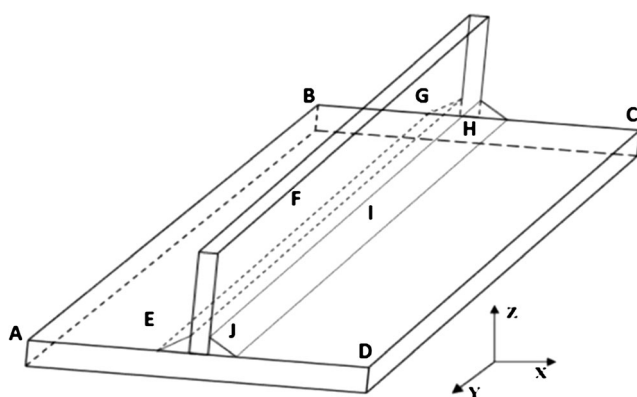


**Fig. 4** Joint geometry of the fillet joint

**Table 6** Welding sequences and their nomenclatures

Welding sequences	Nomenclatures
Points E and J to G and H	WS-I
Points J to H and G to E Point	WS-II
Points F and I to G,H and E,J	WS-III
G, H and E, J to F and I	WS-IV

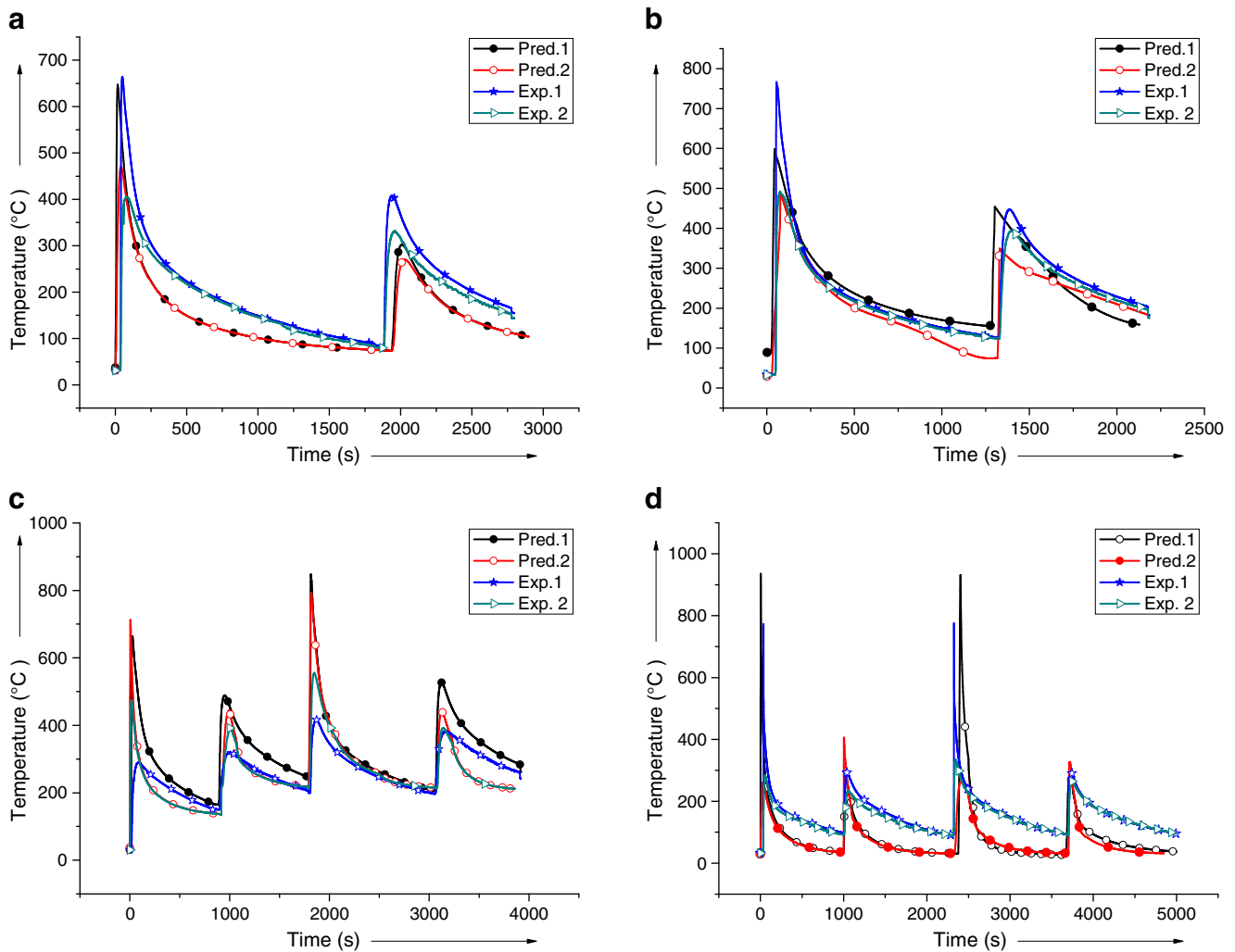


**Fig. 5** a Comparison of predicted and experimental time temperature history for WS-I. b Comparison of predicted and experimental time temperature history for WS-II. c Comparison of predicted and

experimental time temperature history for WS-III. d Comparison of predicted and experimental time temperature history for WS-IV

ples and compared with predicted thermal history. From Fig. 5a–d, it can be observed that the predicted and experimental thermal history are following the same trend and are in reasonable agreement. From Fig. 5 the maximum temperature is observed at the beginning of the weld and it decreases rapidly with time. With distance also the temperature decreases as the maximum temperature is concentrated in the area of heat source only. Four different welding passes went through the same sample; therefore, the temperature raises and cools for four times which depict the variation of the thermal gradients involves during the welding of a multi-pass sample.

The developed model was used to predict the residual stress and angular deformation for four different welding sequences. Figures 6, 8, and 9 show the plot of longitudinal, transverse, and von-Mises residual stress, respectively, in the direction perpendicular to the weld line at the mid length and top

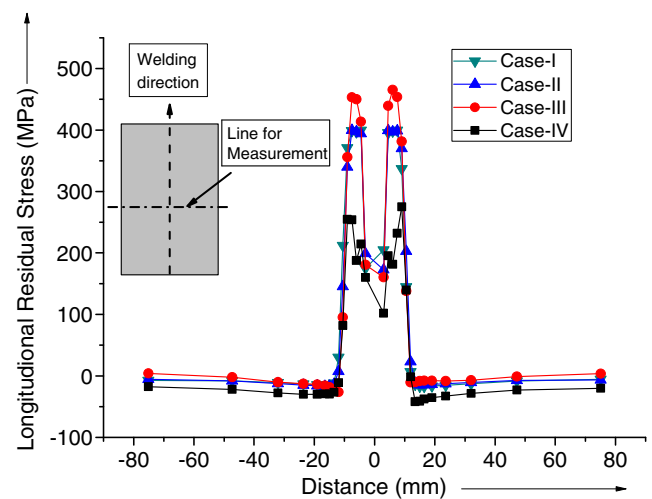


**Fig. 6** Longitudinal residual stress in perpendicular to the welding direction for different welding sequences

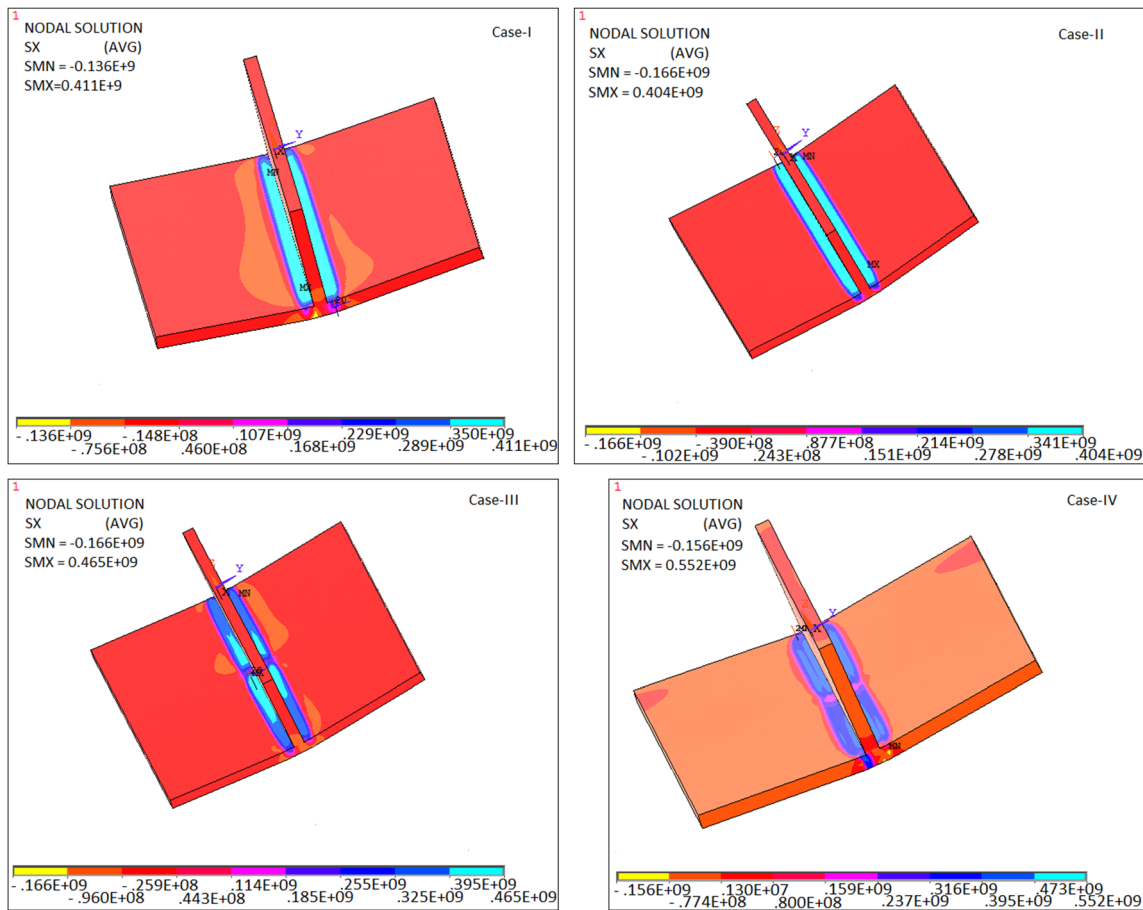


Fig. 7 Contour plot of longitudinal residual stress in perpendicular to the welding direction for different welding sequences

surface of the plate for four different welding sequences. The line of measurement can also be seen from the images.

It can be seen from Figs. 6, 7, 8, and 9 that all the residual stresses are tensile in nature near the weld line and compressive away from the weld line in WS-I to WS-III. But in WS-

IV, transverse residual stress is compressive near and away from the weld line. The residual stress approaches to zero as the distance from the weld line increases. The maximum magnitude of the longitudinal residual stress is more than the transverse one. It has been observed that the maximum 365 MPa and minimum 11 MPa magnitude of von-Mises residual

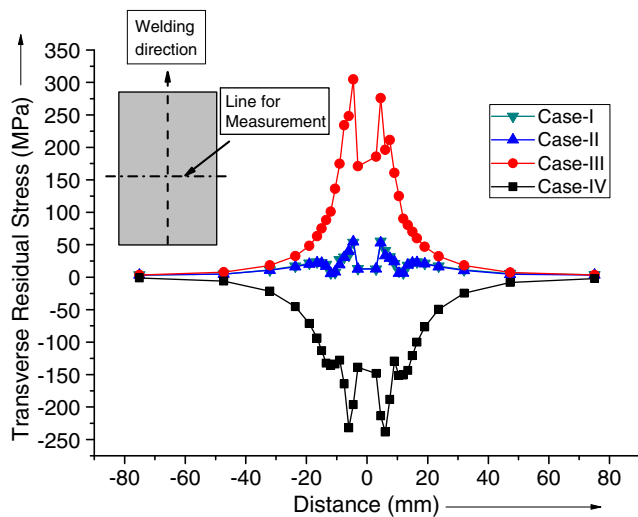


Fig. 8 Transverse residual stress in perpendicular to the welding direction for different welding sequences

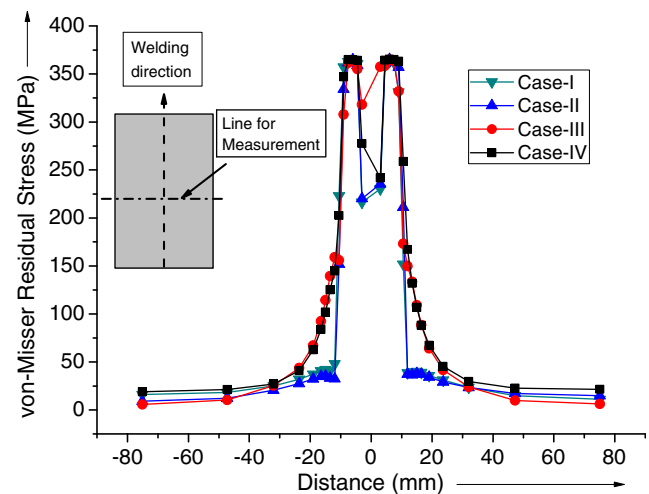


Fig. 9 Von-Mises residual stress distribution



stress has been found in WS-I; maximum 465 MPa magnitude of longitudinal residual stress can be seen at WS-III. Maximum 55.60 MPa magnitude of transverse residual stress can be found at WS-I. During cooling, the weld zone region tries to shrink; this contraction is resisted by the surrounding colder material; therefore, stresses near and within weld region are tensile in nature, but to be in equilibrium, the stresses away from the weld region become compressive in nature because it balances the tensile stress of weld zone region. Figures 7 and 10 show the contour plots of longitudinal and von-Misses residual stress distribution, respectively, for four different welding sequences of double-sided fillet welded joint.

Figure 11 shows the angular distortion patterns perpendicular to the weld line at the mid length of the plate for four different welding sequences. The effect of welding sequences is well prominent. Maximum and minimum values of maximum angular deformation can be seen at WS-II (1.359 mm) and WS-III (0.805 mm), respectively.

The comparison among the maximum and minimum angular deformation value of the weld plates welded using the four different welding sequences are shown in the Table 7. It can be seen that the maximum percentage of error between the predicted and experimental

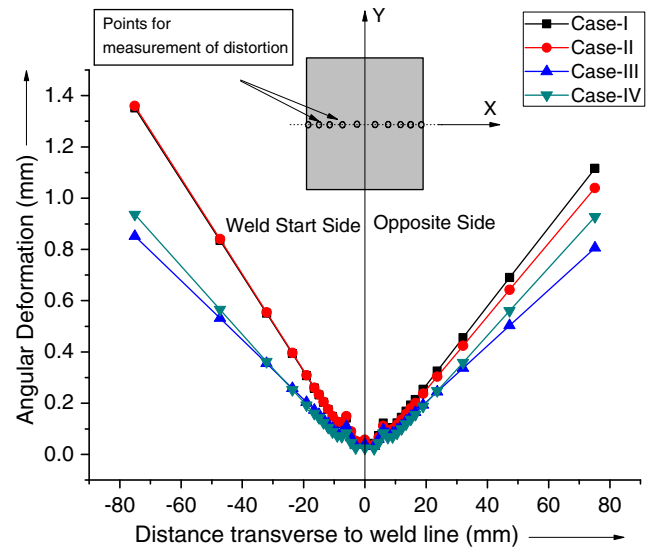


Fig. 11 Plot of angular deformation perpendicular to the weld line

values of angular deformation is 13.14%. Figure 12 shows the plot of experimental angular deformation perpendicular to the weld line. This plot describes the angular change of the fillet joints after complete cooling of the sample which were went through four different

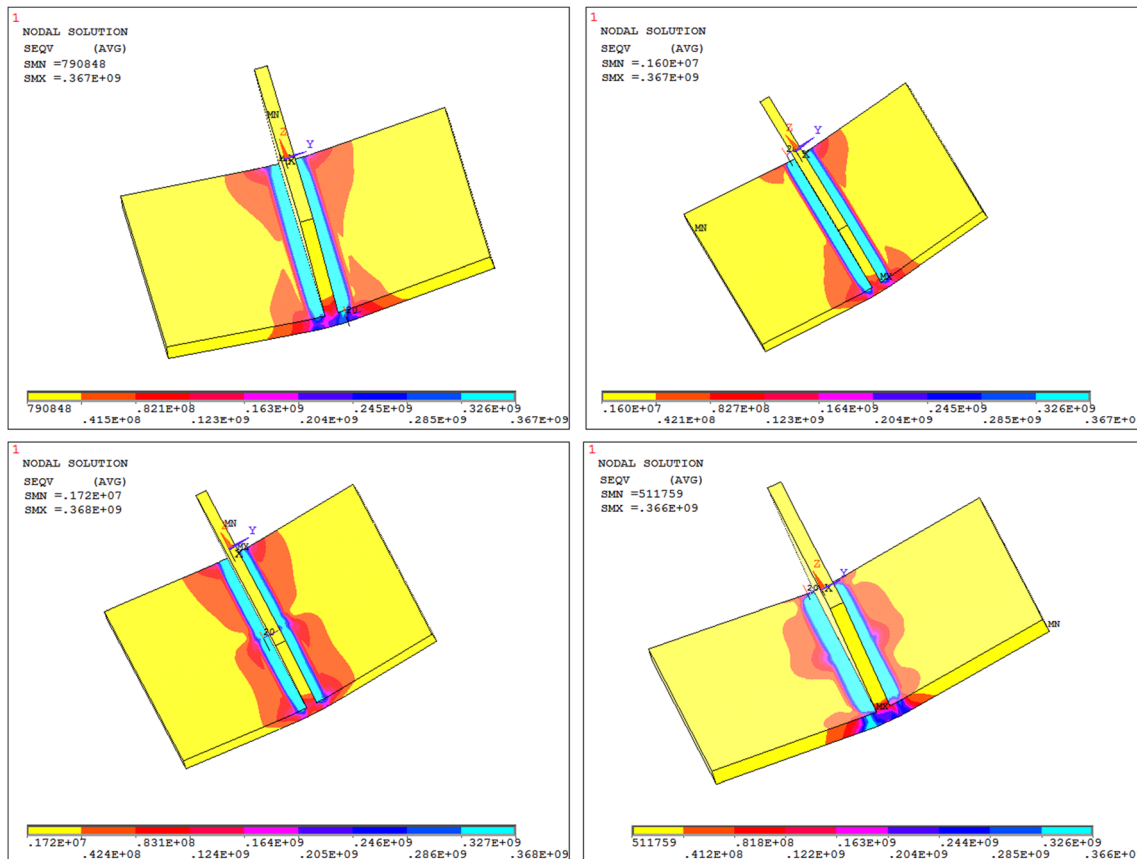


Fig. 10 Contour plot of von-Misses residual stress distribution

**Table 7** Comparison between experimental and predicted maximum angular deformation

	Maximum angular deformation at 75 mm away from weld line (mm)					
	Welding start side (left)			Opposite side (right)		
	Experimental	Predicted	% of Error	Experimental	Predicted	% of Error
WS-I/DS-I	1.254	1.35	7.11	1.047	1.11	6.01
WS-II/DS-II	1.342	1.359	1.25	1.135	1.04	8.37
WS-III/DS-III	0.901	0.851	5.87	0.755	0.8056	6.70
WS-IV/DS-IV	0.813	0.936	13.14	0.825	0.927	12.36

welding sequences. It can be seen that WS-II (1.342 mm) and WS-III (0.7555 mm) give the maximum and minimum values of the angular deformation. The trend of the plots is also well matching with the predicted ones as shown in the Fig. 11. Thus, it can be concluded that the angular deformation in a welded sample can be controlled and minimized by introducing proper welding sequences.

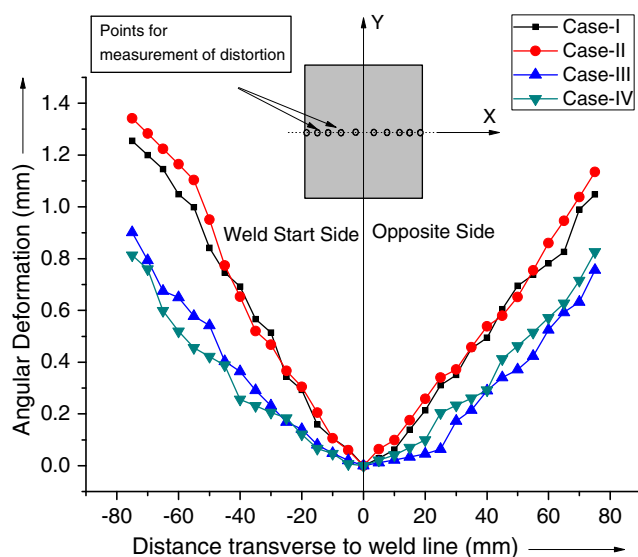
## 5 Conclusions

The residual stresses and angular deformation induced due to different welding sequences in a double-sided fillet joint using submerged arc welding were estimated by means of finite element analysis and experiments. Based on the observations, the following conclusions can be derived from the present investigation:

- A feasible 3-D finite element model for predicting residual stresses and distortions for single- and double-sided fillet

welding have been developed utilizing the nonlinear transient elasto-plastic thermomechanical analysis.

- Experiments have been conducted to measure the thermal history and angular deformation of the different welding sequences. The predicted thermal history and angular deformation profiles are well matching with the experimental ones.
- The residual stress is tensile in nature near and within the weld region, and it is compressive in nature away from the weld region. As the distance from the weld line increases, the stress reaches towards zero. The magnitude of longitudinal residual stress is much higher than that of transverse residual stress.
- Four different welding sequences were considered to perform the FE analysis of double-sided fillet joint. It has been observed that welding sequences have prominent effects on both of distortions and residual stresses. The angular deformation can be reduced if the welding is done following proper welding sequences.

**Fig. 12** Plot of experimental angular deformation perpendicular to the weld line

## References

1. Biswas P, Mandal NR, Das S (2011) Prediction of welding deformations of large stiffened panels using average plastic strain method. *Science and Technology of Welding and Joining* 16(3):227–231
2. Gannon L, Liu Y, Pegg N, Smith MJ (2013) Effect of three-dimensional welding-induced residual stress and distortion fields on strength and behaviour of flat-bar stiffened panels. *Ships and Offshore Structures* 8(5):565–578
3. Khan I, Zhang S (2011) effects of welding-induced residual stress on ultimate strength of plates and stiffened panels. *Ships and Offshore Structures* 6(4):297–309
4. Paik JK, Sohn JM (2012) Effects of welding residual stresses on high tensile steel plate ultimate strength: nonlinear finite element method investigations. *Journal of Offshore Mechanics and Arctic Engineering* 134(2):021401-1–021401-6
5. Yadaiah N, Bag S (2014) Development of egg-configuration heat source model in numerical simulation of autogenous fusion welding process. *Int J Therm Sci* 86:125–138
6. Alberg, H., Simulation of welding and heat treatment modelling and validation, PhD thesis, 2005, Luleå University of Technology, Sweden

7. Tsai CL, Cheng WT (1999) Welding distortion of thin-plate panel structures. *Weld J* (5):78, 156s–165s
8. Tsai CL, Jung GH (2004) Plasticity-based distortion analysis for fillet welded thin-plate T-joints. *Weld J* 83(6):177s–187s
9. Biswas P, Kumar DA, Mandal NR, Mahapatra MM (2011) A study on the effect of welding sequence in fabrication of large stiffened plate panels. *J Mar Sci Appl* 10:429–436
10. Gannon L, Liu Y, Pegg N, Smith M (2010) Effect of welding sequence on residual stress and distortion in flat-bar stiffened plates. *Mar Struct* 23:385–404
11. Kohandehghan AR, Serajzadeh S (2012) Experimental investigation into the effects of weld sequence and fixture on residual stresses in arc welding process. *Journal of Materials Engineering and Performance* 21(6):892–899
12. Perić M, Tonković Z, Rodić A, Surjak M, Garašić I, Boras I, Švaić S (2014) Numerical analysis and experimental investigation of welding residual stresses and distortions in a T-joint fillet weld. *Mater Des* 53:1052–1063
13. Podder D, Mandal NR, Das S (2014) Heat source modeling and analysis of submerged arc welding. *Weld J* 93:183–192
14. Biswas P, Mandal NR (2010) Thermomechanical finite element analysis and experimental investigation of single-pass single-sided submerged arc welding of C-Mn steel plates. *Proceedings of the Institution of Mechanical Engineers, Part B: Journal Engineering Manufacture* 224(B4):627–639
15. Wang J, Ma N, Murakawa H, Teng B, Yuan S (2011) Prediction and measurement of welding distortion of a spherical structure assembled from multi thin plates. *Mater Des* 32:4728–4737
16. Lindgren LE (2001) Finite element modeling and simulation of welding. Part 2: improved material modeling. *J Therm Stresses* 24:195–231
17. Fanous FZI, Maher YA, Wifi SA (2003) 3-D finite element modeling of the welding process using element birth and element movement techniques. *Transactions ASME, Journal of Pressure Vessel Technology* 125:144–150
18. Biswas P, Mahapatra MM, Mandal NR (2009) Numerical and experimental study on prediction of thermal history and residual deformation of double-sided fillet welding. *Proceedings of the Institution of Mechanical Engineers, Part-B* 224:125–134
19. Martin, B. S. (1999) Simulation of welding distortions in ship section, PhD thesis, Department of naval architecture and offshore engineering, Technical University of Denmark
20. Wen SW, Hilton P, Farrugia DDJ (2001) Finite element modelling of a submerged arc welding process. *Journals of Materials Processing Technology* 119:203–209
21. Malik, M. A., Qureshi, E. M., and Dar, N. M. (2007) Numerical simulation of arc welding investigation of various process and heat source parameters, *Failure of Engineering Materials & Structures, UET TAXILA Mechanical Engineering Department* pp. 127–141
22. Sharma A, Chaudhary AK, Arora N, Mishra BK (2009) Estimation of heat source model parameters for twin-wire submerged arc welding. *Int J Adv Manuf Technol* 45:1096–1103
23. Bag S, Kiran DV, Syed AA, De A (2012) Efficient estimation of volumetric heat source in fusion welding process simulation. *Welding in the world* 56:88–97
24. Yadaiah N, Bag S (2012) Effect of heat source parameters in thermal and mechanical analysis of linear GTA welding process. *The Iron and Steel Institute of Japan* 52:2069–2075
25. Stamenković D, Vasović I (2009) Finite element analysis of residual stress in butt welding two similar plates. *Scientific Technical Review* 59(1):57–60
26. Mondal, A. K., Bag, S. and Biswas P. (2013) “3-D finite element analysis of effect of process parameters on residual stresses of saw butt joint”, 7th Asia Pacific IIW International Congress. Singapore, 8–10
27. Mondal, A. K., Ranjan, R., Bag, S., Biswas P. and Mahapatra, M. M. (2012) Finite element analysis of weld induced residual stress of double sided fillet welded joint. 21st International Symposium on Processing and Fabrication of Advanced Materials (PFAM-21), IIT Guwahati, 10–13
28. Adak M, Soares GC Effects of different restraints on the weld-induced residual deformations and stresses in a steel plate. *Int J Adv Manuf Technol* 71(1):699–710
29. Chen, B. Q., Adak, M., and Soares, G. C. (2012) Numerical investigations to study the effect of weld parameters on the temperature-time history in steel plates. *Maritime Engineering and Technology* Edited by Santos T. A. CRC Press, pp. 285–292
30. Nart E, Celik Y (2013) A practical approach for simulating submerged arc welding process using FE method. *J Constr Steel Res* 84:62–71
31. Jiang W, Yahiaoui K, Hall FR (2005) Finite element predictions of temperature distributions in a multipass welded piping branch junction. *Trans ASME Journal of Pressure Vessel and Technology* 127: 7–12
32. Kanjilal P, Pal TK, Majumdar SK (2006) Combined effect of flux and welding parameters on chemical composition and mechanical properties of submerged arc weld metal. *J Mater Process Technol* 171:223–231
33. Liang W, Murakawa H, Deng D (2015) Investigation of welding residual stress distribution in a thick-plate joint with an emphasis on the features near weld end-start. *Mater Des* 67:303–312
34. Kiran DV, Cho D-W, Song W-H, Na S-J (2014) Arc behavior in two wire tandem submerged arc welding. *J Mater Process Technol* 214: 1546–1556
35. Armentani E, Esposito R, Sepe R (2007) The effect of thermal properties and weld efficiency on residual stresses in welding. *Journal of Achievements in Materials and Manufacturing Engineering* 20:319–322
36. Tarnag YS, Juang SC, Chang CH (2002) The use of grey-based Taguchi methods to determine submerged arc welding process parameters in hardfacing. *J Mater Process Technol* 128:1–6
37. Zhao D, Wanga Y, Lin Z, Sheng SM (2013) An effective quality assessment method for small scale resistance spot welding based on process parameters. *Independent Nondestructive Testing and Evaluation International* 55:36–41
38. Shen S, Oguocha INA, Yannacopoulos S (2012) Effect of heat input on weld bead geometry of submerged arc welded ASTM A709 Grade 50 steel joints. *J Mater Process Technol* 212:286–294
39. Nowacki J, Rybicki P (2005) The influence of welding heat input on submerged arc welded duplex steel joints imperfections. *J Mater Process Technol* 164–165:1082–1088
40. Ma N, Li L, Huang H, Chang S, Murakawa H (2015) Residual stresses in laser-arc hybrid welded butt-joint with different energy ratios. *J Mater Process Technol* 220:36–45
41. Akbari Mousavi SAA, Miresmaeili R (2008) Experimental and numerical analysis of residual stress distribution in TIG welding process for 304L stainless steel. *J Mater Process Technol* 208: 383–394
42. Jun T-S, Korsunsky AM (2010) Evaluation of residual stresses and strains using the eigenstrain reconstruction method. *Int J Solids Struct* 47:1678–1686
43. Teng T-L, Fung C-P, Chang P-H, Yang W-C (2001) Analysis of residual stresses and distortions in T-joint fillet welds. *Int J Press Vessel Pip* 78:523–538
44. Brown S, Song H (1992) Implication of three-dimensional numerical simulation of welding of large structures. *Weld J* 71(2):55s–62s
45. Michaleris P, DeBicari A (1997) Prediction of welding distortion. *Weld J* 76(4):172s–180s